Fluorescent core-shell nanoparticles and nanocapsules using comb-like macromolecular RAFT agents: synthesis and functionalization thereof

Chloé Grazon, Jutta Rieger, Patricia Beaunier, Rachel Méallet-Renault, Gilles Clavier

Fluorescent core-shell nanoparticles and nanocapsules using comb-like macromolecular RAFT agents: synthesis and functionalization thereof

Chloé Grazon[a]*, Jutta Rieger[b]*, Patricia Beaunier[c], Rachel Méallet-Renault[a†], Gilles Clavier[a]

Fluorescent nanoparticles and nanocapsules (FNPs) were synthesized *via* a one-pot RAFT miniemulsion process copolymerizing BODIPY-methacrylate and styrene in water. Ultra-bright sub-100 nm core-shell nanoparticles could be obtained with BODIPY covalently linked in the core, and possessing various shells. The nature and architecture of the particle shells could be tuned by using different macromolecular RAFT (macro-RAFT) agents in the miniemulsion polymerization process. The macro-RAFTs were composed of poly(ethylene oxide) acrylate (PEOA) and/or acrylic acid (AA), for their biocompatibility and functionality respectively, in different proportions. Interestingly, with comb-like macro-RAFT agents comprising a high number of PEOA, nanocapsules were formed, while with linear macro-RAFT agents or with those exhibiting a high number of AA, full core-shell nanoparticles were obtained. For all the structures the control of the polymerization, and the physico-chemical properties, such as size and morphology, zeta-potential and photophysic properties were measured and compared with FNPs exhibiting a linear PEO-*b*-PAA block copolymer shell structure (*C. Grazon, J. Rieger, R. Méallet-Renault, G. Clavier, B. Charleux, Macromol. Rapid Commun. 2011, 32, 699*). Regardless of the shell structures, based on estimated brightness, the formed nanoparticles were 100-1000 times brighter than quantum dots. Ultimately, the shell of the different FNPs were successfully functionalized with a second fluorophore via the AA carboxylic acid moieties. Thus, water-soluble ultra-bright FNPs with two fluorophores in distinct environment (water and in polystyrene) were obtained. They should have great potential in bioimaging application.

Introduction

In the last decade, fluorescent molecules and nano-objects have received increasing interest for their high potential in biology and biochemistry. They are especially attractive for sensing, bioimaging and biomedical applications.[1,2] Two main types of fluorescent nanoparticles (FNPs) can be distinguished[3,4]: (1) inorganic intrinsically fluorescent nanoparticles, such as quantum dots[5], and (2) non-fluorescent particles, mostly silica[6] or polymer[7] particles, that are doped with organic fluorophores. Usually, the second type of FNPs is less toxic and more easily functionalizable than the first type. Nevertheless, one of its problems is that the fluorophores can leak out of the matrices' particles with time. In order to avoid this shortcoming, the best solution is to covalently link the fluorophores to the polymer backbone. This can be achieved either by post-modifying the polymer with reactive fluorophores or by copolymerizing fluorescent monomers with a comonomer.[8–10] When bio-imaging applications are targeted, it is crucial to control the nanoparticles' surface properties in order to control their interaction with cells or other bio-surfaces[11], and to functionalize the nanoparticles with specific biomolecules relevant for targeting.[12–16] Fluorescent core-shell polymeric nanoparticles composed of a hydrophobic fluorescent core and a hydrophilic shell can be prepared using Reversible Deactivation Radical Polymerization (RDRP) ~~controlled radical polymerization (CRP)~~ in aqueous dispersed media.[17,18] Recent progress in ~~CRP~~ RDRP in aqueous dispersed media, particularly in RAFT (Reversible Addition Fragmentation chain Transfer) polymerization, has allowed the synthesis of block copolymers particles with multi-functionality in water. Indeed, when reactive soluble polymers instead of surfactants are used in such a process, amphiphilic copolymers are formed that assemble during their synthesis into core-shell nanoparticles. This latter approach was named polymerization-induced self-assembly (PISA).[19,20,21,22,23] It was recently applied to the synthesis of fluorescent core-shell nanoparticles where a free fluorescent dye (Nile Red) was encapsulated in a dispersion polymerization approach performed in methanol.[24] In another study, reactive ketone functions were introduced in the core-shell nanoparticles synthesized by PISA in water, and fluorescein was grafted post-polymerization via hydrazone chemistry.[25] In our previous studies[26,], we have developed a simple surfactant-free one-pot miniemulsion polymerization process in water based on the RAFT mechanism. It allows the controlled synthesis of fluorescent nanoparticles with a hydrophobic core made of polystyrene copolymerized with a BODIPY monomer, and a hydrophilic shell made of a linear poly(ethylene oxide)-*block*-poly(acrylic acid) (PEO-*b*-PAA) diblock copolymer. BODIPY was chosen as fluorophore for its attractive spectroscopic features such as a tunable emission spectrum from green to red and high fluorescence quantum yield. Thanks to its polymerizable methacrylate function, it was covalently linked to the polymer chains to avoid leaking of the fluorophore out of the particle. Poly(ethylene oxide) was selected as steric stabilizer for its biocompatibility and stealth properties[27], and acrylic acids provide carboxylic acid groups available for post-functionalization. A miniemulsion process was mandatory because of the very low solubility of the fluorescent BODIPY monomer (π) in water, inhibiting diffusion through the water phase as would be required in emulsion or dispersion polymerization conditions.[26,29] To form metastable droplets for miniemulsion, amphiphilic triblock copolymers had to be synthesized by chain extension with styrene/π in the bulk prior to the real miniemulsion polymerization step.

In the current study, we were interested in tuning the surface chemistry of the fluorescent nanoparticles, by coating them with either hydrosoluble homopolymers, linear PAA or comb-like poly(poly(ethylene glycol) methyl ether acrylate) (PPEOA), or their random copolymers, P(AA-*co*-PEOA). Compared to our

former study using PEO-*b*-PAA diblock copolymers made in three synthetic steps, those can be obtained more readily (economy of one synthesis step) thanks to a more straightforward synthetic pathway. However, the change in macromolecular RAFT (macro-RAFT) agents' architecture made the adjustment of the polymerization conditions necessary. In the past, Hawkett *et al.*[30,31] had indeed studied the miniemulsion polymerization of styrene and butyl acrylate using PAA-based amphiphilic macro-RAFT agents and they concluded that the molar mass and nature of the hydrophilic PAA and hydrophobic PS segment must be precisely adjusted in order to reach control over the miniemulsion polymerization system. Whereas, PEO[32,33], PAA[34,35], P(AA-*co*-PEOA)[36,37], PMAA[38] or P(MAA-*co*-PEOMA)[39,40]-based macro-RAFT agents have already been successfully used in RAFT emulsion polymerization, to our knowledge, in miniemulsion conditions, *linear* PAA[30,31] and PEO[29,41]-based macro-RAFT agent have been used, but comb-like structures, based on PEOA or/and AA have not been studied yet.

In the first part of the present study, conditions using comb-like PPEOA or P(AA-*co*-PEOA)-based RAFT agents for stabilizing and controlling the miniemulsion polymerization of styrene have been searched. After robust conditions were found, the fluorescent BODIPY phenyl methacrylate (π) was added to the process in order to prepare aqueous dispersions of fluorescent nanoparticles at high solids contents. The second part of the study was then dedicated to the physico-chemical characterization of the particles: the particles' aggregation number, hydrodynamic diameter and morphology, zeta potential and the photophysical properties were determined and compared to the former nanoparticles prepared using the linear PEO-*b*-PAA diblock copolymer as a stabilizing block. Finally, we explored the possibility to post-functionalize the NP's shell by grafting a second fluorophore in order to design nanoparticles which emit at two distinct wavelengths.

Experimental section

Instrumentation

^{1}H NMR spectra were recorded in $CDCl_3$ on a JEOL ECS (400 MHz) spectrometer. All chemical shifts are referenced to Me_4Si (TMS) used as internal standard.

The number-average molar mass (M_n), the weight-average molar mass (M_w), and the molar mass distribution (~~polydispersity index~~ dispersity M_w/M_n, Đ) were determined by size exclusion chromatography (SEC - $M_{n,SEC}$) using THF as an eluent at a flow rate of 1 mL min^{-1}. For analytical purposes, the acidic functions of the block or alternated copolymers were transformed into methyl esters. Therefore, the copolymers were recovered by drying the aqueous dispersions. After dissolution in a THF/H_2O mixture and acidification of the medium with a 1M HCl solution, they were methylated using an excess of trimethylsilyldiazomethane.[42] Polymers were analyzed at a concentration of 5 mg mL^{-1} in THF after filtration through 0.45 µm pore size membrane. The SEC apparatus was equipped with a sample delivery module (GPCmax from Malvern Instruments) and two columns thermostated at 40°C (PLgel Mixed C (7.5 mm × 300 mm), bead diameter: 5 µm). Detection was made with a differential refractive index detector (Viscotek VE 3580 RI detector) and a UV-vis. detector (Waters 486 Tunable Absorbance Detector). The Viscotek OmniSEC software (v 4.6.2) was used for data analysis and the relative M_n and M_w/M_n were calculated with a calibration curve based on polystyrene standards (from Polymer Laboratories).

The *z*-average particle diameter (named D_z) and the particle size distribution (dispersity factor, named σ), were determined by dynamic light scattering (DLS) of the diluted aqueous dispersions, at an angle of 90° at 20°C, with a Zetasizer Nano S90 from Malvern, using a 4 mW He-Ne laser at 633 nm. A value of σ below 0.1 is characteristic of a narrow particle size distribution. All calculations were performed using the Nano DTS software.

Zeta potentials (ζ) were performed on a Zetasizer Nanoseries (Malvern) apparatus at the Institut Curie, Paris, France. Samples were prepared at a concentration of 0.005 wt% diluted with 14mM NaCl water, buffered with 1mM phosphate/citrate salts (pH values varied from 4 to 8). Samples were analyzed in DTS 1060 plastic cells, at 25°C. Three measurements of at least ten scans were performed for each sample.

UV-vis. spectra were recorded on a Varian Cary 5000E (Palo Alto, CA USA) double beam spectrometer using a 10 mm path quartz cell from Thuet (Bodelsheim, France). Fluorescence emission spectra were measured on a SPEX Fluoromax-3 (Horiba Jobin-Yvon). A right-angle configuration was used. Optical density of the samples was checked to be less than 0.1 to avoid reabsorption artifacts. The fluorescence quantum yields Φ_F were determined using Rhodamine 590 (Φ_F = 0.95 in ethanol) as a reference (error of 5 %).[43] The fluorescence decay curves were obtained with a time-correlated single-photon-counting method using a titanium-sapphire laser (82 MHz, repetition rate lowered to 4 MHz thanks to a pulse-peaker, 1 ps pulse width, a doubling crystals is used to reach 495 nm excitation) pumped by an argon ion laser from Spectra Physics (Mountain View, CA USA). For the fluorescent BODIPY-based monomer, π, the Levenberg-Marquardt algorithm was used for non-linear least square fit as implemented in the Globals software (Globals Unlimited, Villa Grove, USA). Lifetimes are given with an error of $\pm$ 0.05 ns. In order to estimate the quality of the fit, the weighted residuals were calculated. In the case of single photon counting, they are defined as the residuals, *i.e.* the difference between the measured value and the fit, divided by the square root of the fit. χ^2 is equal to the variance of the weighted residuals. A fit was said appropriate for χ^2 values between 0.8 and 1.2.

For multi-exponential fluorescent decays (nanoparticles), no fit was attempted and the average fluorescence lifetimes were calculated by integrating the area below the decay curve as:[44]

$$<\tau>=\frac{\int_0^\infty tI(t)dt}{\int_0^\infty I(t)dt} \qquad \textit{Equation 1}$$

Conventional transmission electron microscopy (TEM) was performed on a JEOL JEM CX II UHR microscope operating at 100 keV and equipped with a Keen View CCD camera from Soft Imaging System (Olympus) calibrated with three polystyrene

particle samples (PELCO 610-SET - 91, 300, and 482 nm, Ted Pella Inc.). The acquisition was done with the iTEM software from Soft Imaging System (Olympus). The samples were diluted in water prior to analysis and then deposited on a carbon-coated copper grid.

Materials

Poly(ethylene glycol) methyl ether acrylate (Sigma-Aldrich, M_n = 454 g mol^{-1}), acrylic acid (99 %, Aldrich), 2-methyl-2-[(dodecylsulfanylthiocarbonyl)sulfanyl]propanoic acid (97%, Strem, TTCA), (trimethylsilyl)diazomethane (2.0 M in diethyl ether, Aldrich), 4,4'-azobis(4-cyanopentanoic acid) (Aldrich, ACPA), *N*-(3-dimethylaminopropyl)-*N*'-ethylcarbodiimide hydrochloride (Sigma, EDC), fluoresceinamine (Sigma, FA), ethanolamine (Sigma-Aldrich, EtOA) and ethylenediamine (Sigma-Aldrich, Et$(NH_2)_2$) were used as received. Solvents (Carlo Erba) were of synthetic grade and purified according to standard procedures. Styrene was distilled under reduced pressure. 2,2'-Azobis(2-methylpropionitrile) (98%, Sigma, AIBN) was recrystallized from chloroform containing a few drops of petroleum ether. The synthesis of BODIPY-based fluorescent monomer with a phenyl methacrylate function (π, **Figure SI-1**) was performed as previously described.[26]

Synthesis of fluorescent nanoparticles by RAFT miniemulsion polymerization

The RAFT copolymerization of styrene and π was performed in a one-pot phase inversion process[26], in the presence of a stabilizing P(PEOA-*co*-AA), PPEOA or PAA macro-RAFT agent. Those macro-RAFT agents were synthesised according to our previous study[36], using different amounts of PEOA, AA and the trithiocarbonate-based RAFT agent, TTCA (**Scheme SI-1**). In a typical experiment P($PEOA_{11}$-*co*-AA_{11}) macro-RAFT synthesis, Table SI-1, entry 3), the trithiocarbonate-based RAFT agent, TTCA, (0.80 mmol, 291 mg, MW = 364 g mol^{-1}), acrylic acid (AA, 10 mmol, 720 mg), PEOA (10 mmol, 4.54 g) and DMF (as an internal reference for the ^{1}H NMR determination of the monomer consumption in deuterated chloroform) (4 mmol, 292 mg) were dissolved in 9.9 mL of 1,4-dioxane at room temperature. Then, 0.1 mL of a 0.53 M solution of ACPA in 1,4-dioxane were added. The mixture was purged with nitrogen for 30 min in an ice bath, and then placed in an oil bath thermostated at 80°C to initiate the polymerization. After 90 min, the reaction was stopped by immersion of the flask in iced water. The monomer conversion was determined by ^{1}H NMR in $CDCl_3$. The copolymer was precipitated twice in cold *n*-pentane in order to remove the monomers and dried under reduced pressure..

Then, for a typical experiment of the nanoparticles synthesis (**FNP5**), 197 mg of P($PEOA_{11}$-*co*-AA_{11}) macro-RAFT (3.2×10^{-5} mol, M_n = 6.2 kg mol^{-1}) were dissolved in a mixture of 660 mg of styrene (6.3×10^{-3} mol), 2.0 mg of AIBN (1.2×10^{-5} mol) and 29 mg of monomer π (6.3×10^{-5} mol), in a septum-sealed flask. The mixture was purged with argon for 30 min in an ice bath, and then placed in an oil bath thermostatically controlled at 80°C to initiate polymerization. After 70 min, the reaction was stopped by immersion of the flask in iced water. The conversion of the monomers (styrene and π) was determined by gravimetry and SEC, respectively (for details see below). To the cold organic mixture, 5 mL of a 0.1 M NaOH solution (pH = 12.5) is added. An ultrasonic horn (Bandelin electronics, Sonoplus HD 2200) was then placed in the biphasic mixture cooled down in an ice bath and powered at 130W for 10 minutes.

After the miniemulsion formation, the pH decreased to 11. The miniemulsion was purged with argon for 30 min in an ice bath, and then placed in an oil bath thermostatically regulated at 80°C to reinitiate the polymerization. Sampling was performed at regular time intervals and monomer conversions were determined by gravimetric analysis for styrene corrected from the styrene loss by evaporation during the sonication process (25 wt% calculated by comparison of ^{1}H NMR spectra in $CDCl_3$ and gravimetric analysis[45]) and by SEC using the UV-visible detection at 528 nm for π.

Nanoparticles chains' theoretical number-average molar mass ($M_{n,th}$) were calculated as $M_{n,th} = M_{CTA} + 1/n_{CTA} \times (\chi_S \times m_S + \chi_\pi \times m_\pi)$, were χ_i stands for the individual molar conversion of monomer i, m_i stands for the mass of monomer i used in the synthesis and CTA refers to the chain transfer agent.

Functionalization of the nanoparticles (*e.g.* with fluoresceinamine)

In a typical experiment, 0.3 mL of the pristine nanoparticles aqueous dispersion batch (0.1 g mL^{-1}) was diluted to 4 mL of water in the dark (final concentration = 8 mg mL^{-1}). In parallel, ~ 5 mg of fluoresceinamine (FA, 0.01 mmol) was dissolved in 0.4 mL of ethanol. Once the FA was dissolved, the solution was added to the nanoparticle dispersion and the mixture was vigorously stirred at 4°C. Then, a solution of EDC (15 mg, 0.1 mmol) in water (1 mL) was added to the previous mixture. To quench the reaction, ethanolamine (2.3 µL, 0.04 mmol) was added 2 hours later. The reaction solution was stirred at 4°C for further 12 hours in the dark. Finally, the mixture was transferred in a cellulose ester dialysis membrane (MWCO: 300 kDa, Spectrapor) and dialyzed against water for 7 days in the dark.

The grafting efficiency of FA was quantified by UV-vis spectrometry by comparison of the number of FA with the number of π per FNP. To do so, an absorption spectra of the FNP was recorded in water at pH=8 at room temperature and then the maximum absorption band of the BODIPY (at 528 nm, ε_π = 73×10^3 M^{-1} cm^{-1}[26]) was compared with the one of the FA (at 494 nm, $\varepsilon_{FA,\,grafted}$ = 88×10^3 M^{-1} cm^{-1} at pH 8[46]).

Results & discussion

Synthesis of core-shell polystyrene nanoparticles

Firstly, different water-soluble macro-RAFT agents containing AA and/or PEOA (with molar ratios of AA/PEOA = 100/0, 50/50 and 0/100) were synthesized in dioxane solution in the presence of TTCA as a chain transfer agent (Scheme SI-1, **Table SI-1**). They were named P(AA_x-*co*-$PEOA_y$). In this way, PPEOA and PAA homopolymers, and three P($AA_{50\%}$-*co*-$PEOA_{50\%}$) copolymers with AA/PEOA = 50/50 of different molar mass were obtained.

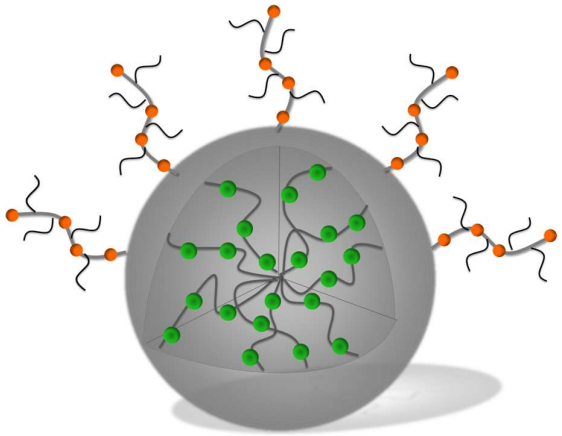

Fig. 1 Schematic representation of the core-shell fluorescent nanoparticles stabilized by P(AA-*co*-PEOA) *comb-like* polymer.

According to our previously published process, the core-shell nanoparticles (**Figure 1**) were then synthesized *via* a one-pot miniemulsion polymerization process in two steps (**Scheme SI-2**). In the first synthesis step, an amphiphilic macro-RAFT agent P(AA_x-*co*-$PEOA_y$)-*b*-PS*0* is prepared through the bulk polymerization of styrene in the presence of the water-soluble macro-RAFT agent. The polymerization is stopped at low monomer conversion and a viscous solution of the amphiphilic diblock copolymer in styrene is obtained. Then, basic water is added and the mixture is sonicated in order to form a miniemulsion of droplets of the remaining styrene that are stabilized by the amphiphilic macro-RAFT agents formed in the previous step.

Core-shell polymeric nanoparticles composed of P(AA_x-*co*-$PEOA_y$)-*b*-PS*0*-PS*1* are finally obtained after 4 hours of polymerization at 80°C, and quasi complete monomer conversion is generally reached. For all experiments, the global molar ratio of styrene to macro-RAFT agent was kept constant and equal to 200, so that the final polymers should all possess polystyrene segments of the same molar mass.

However, by changing the time of the first polymerization step, *i.e.* the bulk step, (while keeping the styrene to macro-RAFT ratio constant), the molar mass of the polystyrene segments PS*0* allowing for the stabilization of the monomer droplets in the miniemulsion polymerization step could be varied. It was thus possible to change the hydrophilic/lipophilic balance of the macro-RAFT without changing the total amount of styrene in the final nanoparticles. It has already been demonstrated[30,31,47] that the hydrophobic segment in the amphiphilic stabilizer has a crucial impact on the particle formation in heterogeneous

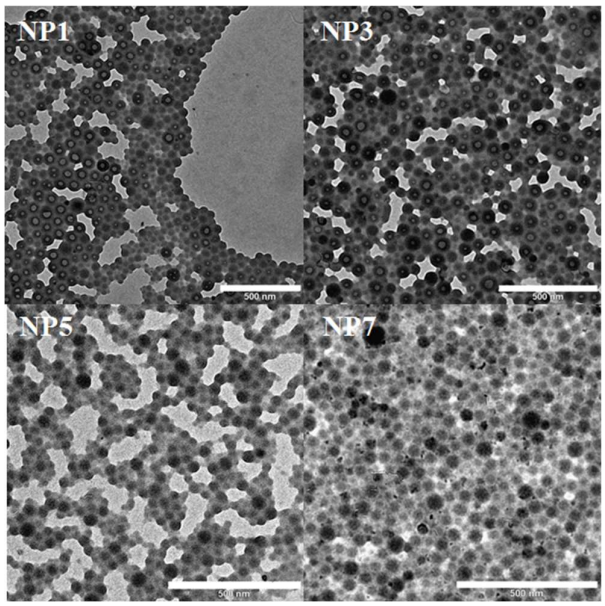

Fig. 2 Transmission electron microscopy images of polystyrene nanoparticles with PPEOA (**NP1**) or P(AA-*co*-PEOA) (**NP3, NP5, NP7**) comb-like shells. Scale bar: 500 nm.

polymerizations and particularly on the control over the polymerization.

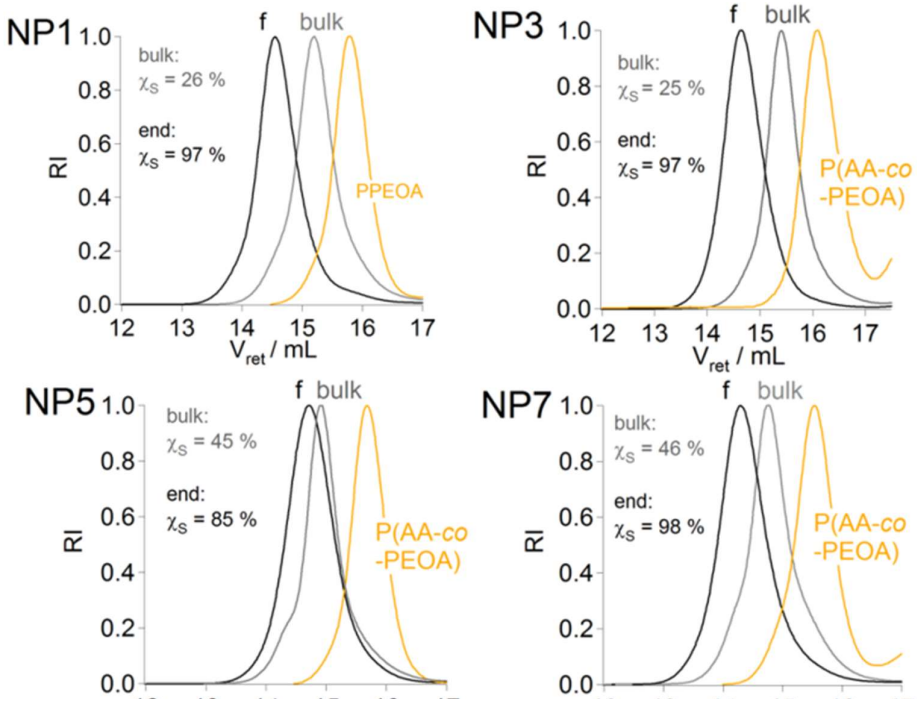

Fig. 3 Size exclusion chromatograms in THF (RI detection) for polymer chains of **NP1, NP3, NP5, NP7** at the beginning of the polymerization (corresponding to the isolated macro-RAFT agent) (— yellow), at the end of the bulk polymerization PS*0* (— grey) and at the end of miniemulsion polymerization **(— black)**.

Table 1 summarizes the syntheses of various polystyrene nanoparticles stabilized by either a PPEOA, P(AA-*co*-PEOA) or PAA, shell. First, the PPEOA macro-RAFT agent with a molar mass of 5.4 kg mol^{-1} was used. This macro-RAFT agent is readily soluble in styrene, which allows performing the above described one-pot miniemulsion process. Stopping the first, bulk polymerization step at different conversion rates, amphiphilic stabilizing PPEOA-*b*-PS*0* copolymers possessing DP_n of PS*0* equal to 40 and 65 were formed (syntheses of **NP1** and **NP2**, respectively). After the miniemulsion polymerization, for both experiments, spherical nanoparticles with a hydrodynamic diameter around 90-95 nm containing a hole in their center were obtained (**NP1** in **Figure 2** and **NP2** in **Figure SI- 2**). They resemble nano-sized vesicles or capsules.

In both cases, the polymerizations were well controlled with molar mass dispersities Đ below 1.37 and molar mass distributions that shifted completely with monomer conversion (SECs traces in **Figure 3**, **NP1** and **Figure SI-3**, **NP2**).

Next, the three comb-like P($AA_{50\%}$-*co*-$PEOA_{50\%}$) macro-RAFT agents with a random distribution of equimolar amounts of AA and PEOA[36] differing in their molar mass (M_n = 3.5, 6.2 and 9.2 kg mol^{-1}) were used. With the shortest macromolecular RAFT agent P(AA_6-*co*-$PEOA_6$) (M_n = 3.5 kg mol^{-1}) and a polystyrene extension of 38 monomer units in the bulk polymerization step, again spherical particles with a diameter of 90 nm with a void in their center were obtained, similar to the experiment using the PPEOA macro-RAFT agents (**NP3,** Figure 2). The polymerization was well controlled with a low molar mass dispersity of 1.29 and no traces of remaining macro-RAFT agent were detected by SEC (**NP3,** Figure 3). With the second, longer macro-RAFT agent P(AA_{11}-*co*-$PEOA_{11}$) (M_n = 6.2 kg mol^{-1}), spherical particles (**NP5)** were also obtained, but they were smaller in size than **NP3** (D_z = 70 nm) and without any void (Figure 2). The polymerization was well-controlled with a dispersity Đ of 1.35, and SEC traces (**NP5**, Figure 3) proved again good efficiency using the P($AA_{50\%}$-*co*-$PEOA_{50\%}$) macro-RAFT agent. The third, longest macro-RAFT agent possessing the highest amount of PEO grafts P(AA_{16}-*co*-$PEOA_{17}$) (M_n = 9.2 kg mol^{-1}) was then tested: with a chain extension of 35 styrene units, the nanoparticles obtained after the miniemulsion polymerization (**NP6**) were polydisperse in size, bigger than the previous ones with a z-average diameter, D_z, of 100 nm. Again, they did not present any holes (**NP6**, **Figure SI-2**). The chain extension took place during polymerization as asserted by SEC, but the dispersities were higher, in the range of 1.6 (Figure SI-3). A former study had related the heterogeneity in particle size to an insufficient length of the hydrophobic PS segment necessary to durably localize the amphiphilic stabilizer at the styrene droplet/water interface.[30,31] We thus performed a second experiment with P(AA_{16}-*co*-$PEOA_{17}$), in which a longer hydrophobic, anchoring PS*0* segment was prepared in the bulk polymerization step. Indeed, using a macro-RAFT agent chain extended by 70 styrene units in average (instead of 35, **NP7** *vs.* **NP6**), the resulting nanoparticles were much more homogeneous in size (**NP7**, Figure 2) and the polymerization was well controlled with low molar mass dispersities (Đ = 1.36), and no remaining macro-RAFT agent was detectable in the SEC traces (**NP7**, Figure 3). Finally, we intended synthesizing nanoparticles with a pure linear poly(acrylic acid) shell using the same procedure. A hydrophilic macro-RAFT agent (PAA_{35}, M_n = 2.9 kg mol^{-1}) possessing a total number of monomer units similar to P(AA_{16}-*co*-$PEOA_{17}$, DP_n = 33) was first synthesized to stabilize the

Table 1 Experimental results of core-shell (fluorescent) nanoparticles. Nanoparticles were synthesized at 80°C using the one-pot procedure, with macro-RAFT agents and stopped after 4h ($[S]_0$ = 1.3 mol L^{-1} H_2O, $[S]_0/[RAFT]_0$ = 200, $[RAFT]_0/[AIBN]_0$ = 3, [NaOH]/[AA]=1.3, pH ≈ 12.5).

NP	macroRAFT agent	n_π[a]	t_0[b], min	$\chi_{S,0}$ [b,c], %	DP_n (PS_0)[b]	$\chi_{S,f}$ [d,e], %	$\chi_{\pi,f}$ [d,e], %	$M_{n,th}$ / kg mol^{-1}	$M_{n,SEC}$, kg mol^{-1}	$Đ = M_w/M_n$	D_z (σ), nm	Void?
NP1	$PPEOA_{11}$	0	90	20	40	97	-	20.6	21.5	1.29	95 (0.03)	√
NP2	$PPEOA_{11}$	0	150	33	65	75	-	17.0	15.7	1.37	90 (0.10)	√
FNP2	$PPEOA_{11}$	1.3	150	26	51	84	98	19.4	18.3	1.43	110 (0.18)	√
NP3	$P(AA_6$-*co*-$PEOA_6)$	0	70	24	38	97	-	18.9	18.7	1.29	90 (0.07)	√
FNP3	$P(AA_6$-*co*-$PEOA_6)$	1.8	80	14	27	100	97	18.2	19.6	1.29	85 (0.19)	√
NP5	$P(AA_{11}$-*co*-$PEOA_{11})$	0	150	45	69	85	-	19.7	17.1	1.35	70 (0.12)	0
FNP5	$P(AA_{11}$-*co*-$PEOA_{11})$	1.9	150	41	66	94	97	22.4	18.5	1.40	85 (0.10)	0
NP6*	$P(AA_{16}$-*co*-$PEOA_{17})$	0	75	18	35	99	-	30.0	27.7	1.56	100 (poly)	0
NP7	$P(AA_{16}$-*co*-$PEOA_{17})$	0	150	46	70	98	-	26.8	24.4	1.36	110 (0.14)	0
NP8	PAA_3	0	90	20	15	100	-	14.0	16.3	1.36	95 (0.10)	0
NP9**	PAA_{35}-*b*-PS_{19}	0	-	-	19	90	-	20.4	27.8	1.84	65 (0.06)	0

* This experiment was conducted with a ratio $[S]_0/[RAFT]_0$ = 240. ** For this experiment it was not possible to use the "one-pot" procedure since the macro-RAFT agent PAA_{35}-TTC is not soluble in styrene. So a first amphiphilic macro-RAFT agent was synthetized and isolated to further initiate the RAFT miniemulsion polymerization. [a] Average number of BODIPY monomer per polymer chain. [b] Time 0 refers to bulk polymerization : respectively end of bulk polymerization (t_0), conversion of styrene ($\chi_{S,0}$) and degree of polymerization, DP_n, of PS block (PS_0). [c] Styrene conversion determined by gravimetry[26]. [d] End of miniemulsion polymerization. [e] BODIPY monomer (π) conversion determined by SEC using the UV-vis. detection.

particles during the miniemulsion polymerization. Nevertheless, this PAA macro-RAFT agent was not soluble in the styrene phase and the developed two steps bulk polymerization-phase inversion process could thus not be applied. Because of the insolubility of PAA_{35} in styrene, we performed the chain extension of polystyrene (19 units) in solution (in 1,4-dioxane at 80°C), isolated the amphiphilic macro-RAFT agent and then used it as a stabilizer and control agent in the miniemulsion polymerization. This macro-RAFT agent possesses a large number of acrylic acid units (35) and should *a priori* provide very efficient electrostatic repulsion at the miniemulsion polymerization pH of 12. Actually, spherical, full nanoparticles (**NP9**) could be obtained, which possessed the smallest average diameter of the series (65 nm) (**NP9**, Figure SI-2). However, the control of the polymerization was limited, with higher molar mass dispersities and final molar masses slightly higher than the theoretically expected values. In order to overcome the problem of solubility of the PAA_{35} macro-RAFT agent, and to avoid the synthesis in dioxane solution and purification step of the amphiphilic macro-RAFT agent, a small oligo-RAFT agent of only 3 units of acrylic acid was also prepared. This macro-RAFT agent was readily soluble in styrene so that the polymerization of styrene could be performed in bulk. At the end of the bulk step, a PAA_3-*b*-PS_{15} macro-RAFT agent was obtained and used in the miniemulsion polymerization step. Full particles (**NP8**) were again obtained, which were however quite heterogeneous in size (**NP8**, Figure SI-2). Nevertheless the polymerization was well controlled (Đ = 1.36) and no macro-RAFT agent was detected in the SEC chromatograms (**NP8,** Figure SI-3).

Partial Discussion. As described above, various core-shell nanoparticles with comb-like hydrophilic shells composed of PEOA and/or AA were synthesized using a one-pot surfactant-free miniemulsion process. It appeared that the nature of the corona and the length of the polystyrene block PS*0* of the

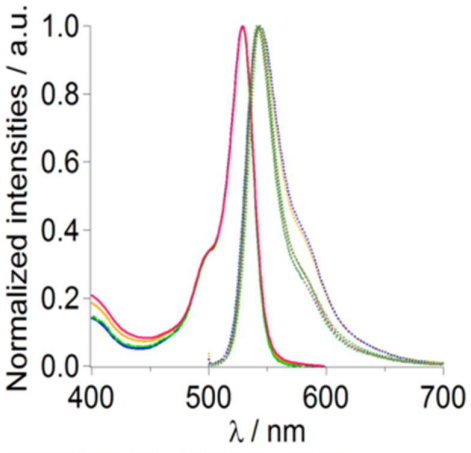

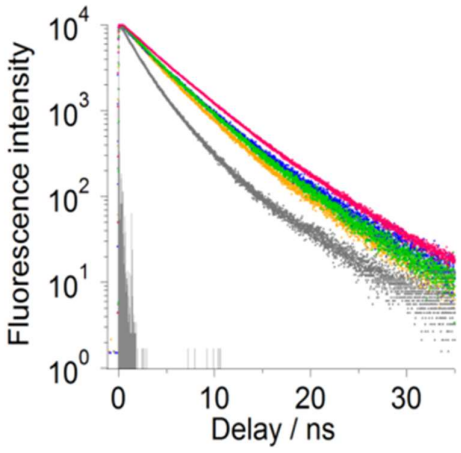

Fig. 4 Spectr **FNP11** (— green)), recc line is the instrument response function, λexc = 495 nm, λf = 545 nm).

amphiphilic macro-RAFT agent (used as both a control agent and a stabilizer in the miniemulsion step) had an influence on the control over the polymerization and on the morphology[48] of the objects. With the long, highly hydrophilic macro-RAFT agent P(AA_{16}-*co*-$PEOA_{17}$) comprising a short polystyrene PS*0* segment formed in the bulk polymerization step (**NP6**), particles were very heterogeneous in size and the polymerization was not well controlled. In contrast, the experiment conducted with the same P(AA-*co*-PEOA) macro-RAFT agent, but possessing a longer polystyrene PS*0* segment showed a good control over the polymerization (**NP7**). Good control over polymerization was also obtained using the macro-RAFT agents with lower molar masses, $PPEOA_{11}$, P(AA_{11}-*co*-$PEOA_{11}$) and P(AA_6-*co*-$PEOA_6$). A plausible explanation for the loss of control in experiment **NP6** exhibiting a short PS*1* segment relative to P(AA-*co*-PEOA), might be that in this case the localization of the macro-RAFT agent at the monomer droplets/water interphase is rather dynamic. Thus, this macro-RAFT agent should exhibit a preference for the water phase compared to the interface of the styrene droplets/particles. Consequently, particle stabilization is less efficient, yielding higher particle size dispersity, and a loss of control over the polymerization.[20,49] In conclusion, with respect to the molar mass of the hydrophilic segment, a sufficiently long polystyrene block PS*0* must be attached in the bulk polymerization step in order to reach control over polymerization. Similarly, Hawkett *et al.* had used amphiphilic PAA_5-*b*-PS_y-TTC-C_4 macro-RAFT agents with polystyrene blocks of variable lengths in the miniemulsion polymerization of styrene.[30,31] They observed that the polymerization was best controlled with the macro-RAFT agents possessing the longest hydrophobic PS segment (y = 24). They explained that only the most hydrophobic PAA_5-*b*-PS_y-TTC-C_4 were completely anchored at the styrene droplets/water interface, thus preventing droplets from coalescence and Ostwald ripening.

Another parameter which apparently affected the polymerization mechanisms is the presence or absence of PEOA in the macro-RAFT agent: it seems responsible for changes in particle morphology. Particles prepared without PEOA in the macro-RAFT (**NP8** and **NP9**) do not possess any voids. In contrast, particles obtained with homopolymer PPEOA (**NP1**) possess one hole in the center, just as nanocapsules do. In the past, multiple holes have already been observed in PS particles when PEO was present in the macro-RAFT agent used in the emulsion[50] and miniemulsion[31] polymerization of styrene. PPEOA or other PEO-based polymers are soluble in both the water phase and the styrene phase, while deprotonated PAA is only soluble in the basic water phase. As such, PPEOA-*b*-PS might be located both at the droplet interface and in the growing polymer particle, *loci* of the polymerization. Nanoparticles formed with the *comb-like* copolymer P(AA_x-*co*-$PEOA_y$)-*b*-PS macro-RAFT agent containing the lowest number of AA possess a hole in their center, while those formed with 11 or 16 AA units do not. In our previous study, it had already been observed that a small fraction of the polystyrene particles synthesized using a PEO_{45}-*b*-PAA_{15}-*b*-PS_{25} macro-RAFT agent possessed holes in their center.[26] Again, this might be explained by the differences in solubility: for low weight fractions of acrylic acid, the macro-RAFT agent is soluble in both water and the organic styrene phase, which should favor the formation of double emulsions. At the high pH of the miniemulsion (pH 12), the increase of the AA fraction certainly reduces the solubility of the macro-RAFT agents in the styrene phase, and therefore prevents the formation of double emulsions resulting in the formation of plain full particles.

Fluorescent nanoparticles

Nanoparticles **NP2**, **NP3** and **NP5** were homogenous in size and polymerizations were well controlled (experimental molar masses that correspond to the theoretical ones and Đ < 1.4). Moreover, **NP3** and **NP5** possess multiple carboxylic acids groups in their P(PEOA-*co*-AA) shell that might be used for further grafting of small molecules. Their synthesis conditions were therefore selected as starting points for the synthesis of the corresponding fluorescent particles. In order to prepare fluorescent nanoparticles of the same structure (**FNP2, FNP3** and **FNP5**), BODIPY methacrylate (π), the fluorescent monomer of choice (Figure SI-1), was simply added to styrene in the bulk polymerization step, and then the miniemulsion polymerization was performed according to the protocols established for the non-fluorescent nanoparticles.

Table 2 Physico-chemical properties of FNP with different shells, recorded in water at RT.

					Fluorescence properties					TEM		
Shell	FNP	n_π[a]	[π][b], mol L_S^{-1}	N_π[c]	Φ_F	<τ>[d], ns	$\Delta_{1/2}$[e], cm^{-1}	B[f], L cm^{-1} mol^{-1}	D_z (σ)[h], nm	D_{TEM}[i], nm	N_{Agg}[g]	D[j], chains nm^{-2}
$PPEOA_{11}$	FNP2	1.3	0.08	-	0.58	4.9	970	-	110 (0.18)	-	-	-
P(AA_6-*co*-$PEOA_6$)	FNP3	1.8	0.13	-	0.44	4.2	1230	-	85 (0.19)	-	-	-
P(AA_{11}-*co*-$PEOA_{11}$)	FNP5	1.9	0.10	1960	0.52	4.5	1300	7.4	85 (0.19)	37	1030	0.24
PEO_{45}-*b*-PAA_{15}*	FNP10	2.1	0.17	3680	0.24	3.2	980	6.4	80 (0.15)	40	1750	0.35
PEO_{45}-*b*-PAA_{15}*	FNP11	1.1	0.08	1930	0.39	4.3	980	5.5	75 (0.12)	40	1750	0.35

[a] Average number of BODIPY monomer per polymer chain. [b] Molar concentration of BODIPY monomer per liter of styrene. [c] N_π Average number of π per nanoparticles determined using equation SI-3 [d] Average decay time, determined using equation 1 (λ_{exc} = 495 nm, λ_F = 543 nm). [e] Fluorescence spectra full width at half maximum ($\Delta_{1/2}$). [f] Nanoparticles brightness. [g] Aggregation number determined by TEM using Equation SI-4. [h] z-average particle diameter measured by DLS. [i] FNPs'core diameter estimated by TEM. [j] density of the polymer chains on the FNPs' surface (Equation SI-4). * Already published results[26,52]

Table 3 Physico-chemical characteristics of pristine or grafted (fluorescent) nanoparticles recorded in water. Zeta potentials (ζ) were recorded in phosphate/citrate buffers ([phosphate/citrate] = 1mM, [NaCl] = 14mM).

				ζ / mV					
Exp	NP	Shell structure	Amine[a]	pH 4	pH 5	pH 6	pH 7	pH 8	FA/FNP[c]
-	NP5		-	-12		-26	-28	-24	-
NP5- NH_2-	NP5		$Et(NH_2)_2$	+10	+2	-15		-16	-
NP5- FA	NP5	comb-like	FA + EtOA	-1		-18		-21	-
-	FNP5		-	-16		-29	-36	-30	-
FNP5-FA	FNP5		FA + EtOA	+5		-12	-16	-21	520
-	NP11		-	n.d.[b]	n.d.[b]	-16	-17	-17	-
NP11- NH_2	NP11		$Et(NH_2)_2$	+5	-2	-11	-15	-14	-
NP11- FA	NP11	linear	FA + EtOA	-9		-14		-14	-
-	FNP11		-	n.d.[b]	n.d.[b]	-17	-14	-16	-
FNP11- FA	FNP11		FA + EtOA	-11			-15	-15	1230

[a] Amine grafted on the (F)NP shell. [b] n.d. = not determined (The measurement of the zeta potential at that pH was impossible since the nanoparticles precipitated). [c] Average number of fluoresceinamine (FA) grafted per fluorescent nanoparticles determined by absorption using the relative intensity of FA and π ($\varepsilon_\pi = 73\times10^3 M^{-1}.cm^{-1}$[26] $\varepsilon_{FA,\ grafted} = 88\times10^3 M^{-1}.cm^{-1}$ at pH 8[44]).

FNP2, **FNP3** and **FNP5** were synthesized with the same molar concentration of π (about 1% relative to styrene) (Table 1). At the end of the miniemulsion polymerization, for all FNPs, the molar conversion of π was higher than 97%. SEC analyses (**Figure 5, Figure SI-4**) revealed that the addition of π did not perturb the polymerization control: molar mass control and low molar mass dispersities Đ were maintained for all fluorescent NP (**FNP2**, **FNP3** and **FNP5**). Furthermore, the UV-vis. SEC detection (λ = 528 nm) superposed with the RI trace, which means that the whole polymer distribution contained BODIPY.

Both types of particles (with or without π) had the same morphology (Figure 5, **Figure SI-5**) and were comparable in size. So, including approximately 1 mol% (*i.e.* 5 wt%) of π with respect to the polystyrene polymer chain in the miniemulsion process did not disturb the polymerization mechanism, independently of the macro-RAFT agent used. The developed one-pot miniemulsion polymerization conditions are thus robust for the synthesis of fluorescent nanoparticles with various hydrophilic shell structures.

UV-vis. absorption spectra of FNPs shows the same absorption band as a single π monomer in toluene (**Figure 4**), which is one more proof for the incorporation of π in the FNPs and the chemical integrity of the fluorophore after the radical polymerization.

However, the fluorescence emission spectrum differs from one structure of FNP to the other. For all FNPs, the full width at half maximum (FWHM) in absorption spectra is the same whatever the FNP ($\Delta_{1/2\ abs}$= 937 cm^{-1}) while the FWHM in emission ($\Delta_{1/2}$) is larger **(Table 2).** Usually such effect is attributed to a decreased rigidity in the excited state.[51] Such effect is even more pronounced for **FNP3** and **FNP5** compared to **FNP2**. It seems that the structure of those nanoparticles/nanocapsules leads to a loose excited state. This might be interpreted in terms of environment (structure of the shell, density of the FNP polystyrene-based core) since the parent monomer dye is the same whatever the FNP.

In our previous studies using linear PEO_{45}-*b*-PAA_{15} **(Scheme SI-3**) and approximately 1.1 π per polymer chain (Table 2, **FNP11**)[26,52], nanoparticles with a fluorescence quantum yield of 0.39 could be obtained in water (while the quantum yield of the π monomer is 0.69 in toluene). It has also been observed that an increase in the π concentration from one fluorophore (**FNP11**) to two fluorophores π (**FNP10**) per polymer chain, decreased significantly the fluorescence quantum yield Φ_F from 0.39 to 0.24 and the lifetime from 4.3 ns to 3.2 ns. Moreover, we had demonstrated the greater reactivity of π compared to styrene, leading to a gradient of composition in the polymer chain with a higher density of the fluorophore π near the hydrophilic shell and a lower density in the middle of the hydrophobic core.[26] The observed decrease of Φ_F was thus attributed to the formation of non-fluorescent aggregates along the polymer chain *and* between polymer chains in the particle core. In the present study using a comb-like stabilizing corona, **FNP2**, **FNP3** and **FNP5** contain between 1.3 and 1.9 π fluorophores per polymer chain. Compared to our previous study, they exhibit higher Φ_F of 0.58, 0.44 and 0.52, respectively, and longer fluorescent lifetimes of 4.9, 4.2 and 4.5 ns (Table 2, Figure 4). This interesting result can only be the result of the change in macromolecular architecture of the stabilizing shell, as both types of fluorescent particles are composed of the same polymers (PEO, PAA, PS) and contain both π as a fluorophore. It is well-known that the presence of carboxylic acids close to BODIPY fluorophores can decrease their fluorescence efficiency.[53] In the former *linear* PEO_{45}-*b*-PAA_{15} block copolymer particles (**FNP10 and FNP11**), carboxylic acids adjoined the hydrophobic PS core of the nanoparticles and thus the fluorescent monomer units. In contrast, in **FNP2**, **FNP3** and **FNP5** the hydrophilic shell is made of *comb-like* copolymers of acrylic acids and PEOA, and consequently the π monomers (in the core) should be spatially separated (by the PEO copolymer brush) from most of the carboxylic acids groups. Moreover, the packing of the polymer chains in the particles might be considered: for the FNPs without any voids the aggregation number (N_{agg}, Equation SI-1) and the density of the polymer chains on the FNPs' surface (d, Equation SI-4) can be estimated. The results are displayed in Table 2. Interestingly, for the FNPs

with a P(AA_{11}-*co*-$PEOA_{11}$) shell (**FNP5**), N_{agg} and d were respectively 40% and 30% times lower than for the FNPs with a shell of PEO_{45}-*b*-PAA_{15} (**FNP10**). This result might be explained considering the bulkiness of the PEOA macromonomer, which makes the hydrophilic shell a cumbersome brush type polymer compared to the tight linear PEO-*b*-PAA copolymer. Consequently, the polymer chains in **FNP10** should be more tightly packed than in **FNP5**, which might favor the formation of π inter-chains aggregates at the periphery of the hydrophobic core. This is conform with the fact that the fluorescence emission spectra of "*linear* shell" FNP is narrower than the one of "*comb-like* shell" FNPs, proving that the environment of the π monomer in the first type of FNP is more dense. In conclusion, we thus believe that it is for these two reasons (steric hindrance of the shell due to a difference in the macromolecular architecture and the presence of the carboxylic acids near the surface) that the fluorescence efficiency changes with the chemical nature and especially macromolecular architecture of the particle shell.

Thanks to the aggregation number, the number of fluorophores π per particle (N_π, Equation SI-3) could be estimated. For **FNP5** and **FNP10** with a PS core of about 40 nm in diameter‡, the number of π is respectively 1960 and 3680. Ultimately, the important parameter for fluorescent bio-imaging is the total brightness of the FNP which is given by:

$B=N_\pi \times \varepsilon_\pi \times \Phi_F$ *Equation 2*

where N_π is the number of π per particle, ε_π the molar coefficient extinction of π at 528 nm, and Φ_F the quantum yield of the FNPs.

For a single π in toluene, the brightness is equal to 5.0×10^4 cm^{-1} M^{-1}. In our previous studies, we found that the brightness of **FNP10** (Table 2) was 1300 times higher than a single BODIPY monomer π. Here, the brightness of the new **FNP5** is 1500 times higher than one π. Thus, even if **FNP5** contains around twice less π per nanoparticle, they are brighter than **FNP11** (which is due to the less dense morphology of the FNP leading to a higher Φ_F). Generally, quantum dots with a core made of CdSe, CdS, or CdTe emitting between 370 and 750 nm have a brightness between 6×10^4 and 6×10^5 cm^{-1} M^{-1}.[3] Thus, the synthesized FNPs are approximately 100-1000 times brighter than usual quantum dots if the estimated experimental brightness are compared. As such, those FNPs are among the brightest polymer-based fluorescent nanoparticles synthesized at the day according to Klymchenko *et al*. study[10], which makes them very powerful candidates for imaging.

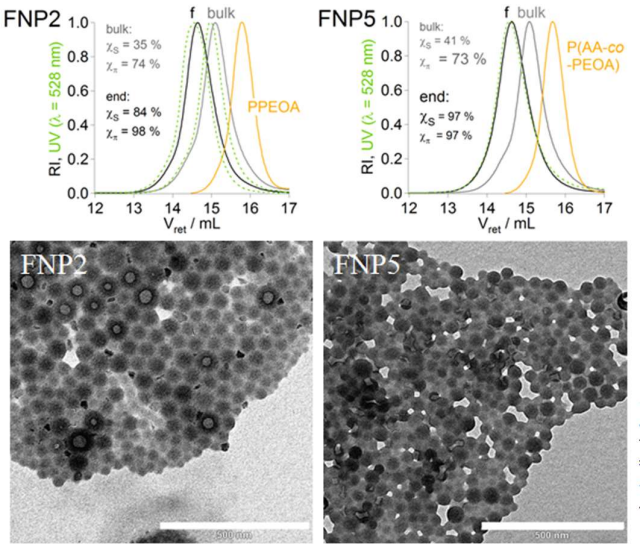

Functionalization of the FNPs

Functionalized fluorescent nanoparticles[13–15] are of particular interest for biomedical applications. Generally, nanoparticles are functionalized thanks to reactive groups, such as thiols, amines, and acids, present on the NP surface. The fluorescent nanoparticles and their non-fluorescent models (**(F)NP2**, **(F)NP3**, **(F)NP5** and **(F)NP11**) all possess carboxylic acids units in their shell, but they are differently distributed along the polymer chain, *i.e.* in the shell. **(F)NP2** exhibits a single carboxylic acid at its outmost α-chain extremity originating from the RAFT agent's (TTCA) R leaving group (Scheme SI-1). In contrast, **(F)NP3** and **(F)NP5** possess carboxylic acids randomly distributed in the bulky P(AA-*co*-APEO) shell. Finally, **(F)NP11** possess a block of poly(acrylic acid) located between the PEO segment and the hydrophobic core of the nanoparticles.

In order to evaluate the impact of the shell architecture on grafting efficiencies, ethylenediamine ($Et(NH_2)_2$) was first grafted as a model molecule (via the formation of activated esters of AA with EDC) (**Table 3**).[54,55] **NP5** and **NP11** were selected for those preliminary grafting experiments since they possess a similar number of carboxylic acids units, but a *comb-like* and *linear* architecture, respectively. In order to rapidly evaluate if the grafting took place or not, the zeta potentials (ξ, Table 3) of the nanoparticles were measured at different pH (pH = 4, 5, 6, 7 and 8). Whatever the pH, for the pristine **NP5** and **NP11** dispersions, negative zeta potentials were measured. Actually, above pH = 5, acrylic acids are at least partially deprotonated, and PEO-coated nanoparticles give generally negative zeta potentials[55]. Interestingly, **NP11** nanoparticle dispersions prepared with the *linear* PEO-*b*-PAA diblock copolymer precipitated below pH = 5[26], whereas the corresponding *comb-like* **NP5** did not. Again, the shells' macromolecular bulky architecture, where AAs are randomly distributed between bulky PEO grafts, should be responsible of the observed differences. Indeed, it is well known that PAA (in its protonated form, *i.e.* generally at pH below the pK_a around 5) can form hydrogen-bonded complexes with PEO segments.[57] Thus, at pH = 5, the PAA intermediate block of **NP11** can form hydrogen bonds with the PEO block and lead to particle aggregation. In contrast, in **NP5** the carboxylic acid groups are randomly distributed in the shell polymer chain, and the steric stabilization by the evenly distributed PEO grafts should inhibit destabilization. Interestingly, after grafting with $Et(NH_2)_2$, *linear*

NP11 (**NP11-NH_2**) particle dispersions remain colloidally stable at pH below pH 5, which is a first proof of grafting. Moreover, their zeta potential becomes positive at pH 4, certainly because of the amino groups that are now present in the shell. *Comb-like* **NP5-NH_2** nanoparticles have a slightly higher zeta potential compared to **NP5**, whatever the pH. As for **NP11** the zeta potential becomes positive for low pH (pH = 4 and 5). The variation of zeta potential before and after grafting and also at different pH is more pronounced for *comb-like* **NP5** than for *linear* **NP11**, which might be explained by the more efficient screening of the PAA part by the dense linear PEO outer shell in **NP11** (Scheme SI-3).

Following these encouraging preliminary results with ethylenediamine, fluoresceinamine (FA) was grafted on **FNP2**, **FNP5** and **FNP11** under the same conditions. The number of FA per nanoparticle could easily be calculated after grafting by comparing the absorption band of the BODIPY (maximum at 528 nm) with the one of the FA (maximum 494 at nm) in basic conditions ($\varepsilon_\pi = 73\times10^3$ M^{-1} cm^{-1}[26], $\varepsilon_{FA,\ grafted} = 88\times10^3$ M^{-1} cm^{-1} at pH 8[46]), knowing the number of BOPIDY fluorophores per particle, N_π. It was determined that *comb-like* **FNP5-FA** possessed in average 520 FA per nanoparticles, while *linear* **FNP11-FA** were functionalized by 1230 FA in average (Table 3). Those results indicate that for both **FNP5** and **FNP11**, 5 % of the carboxylic acids were functionalized. Similar grafting efficiencies were also measured for NP5 and NP11 when the grafting was performed with ethanolamine (respectively 56 ±3% and 62 ±4% of the acid functionalized, determined by elementary analysis, using O and N on 15 mg of dried NPs).[58] The zeta potential of *comb-like* **FNP5-FA** is strongly dependent on pH (positive at pH = 4), while the zeta potential of **FA-FNP11** is negative over the whole range of pH, probably because the fluorescein and the remaining acrylic acids are screened by the linear outer PEO segment.[56] These results demonstrate that the two types of nanoparticles have the same reactivity towards amines regardless of the shell architecture. The overall poor grafting efficiency with fluoresceinamine may be due to its steric hindrance and the electrostatic repulsion between the charged carboxylic acids and FA (both negatively charged at the pH of the reaction).

With the same strategy, it was not possible to graft FA on **FNP2** particles, which possess only one carboxylic acid located at the chain end of the corona polymers. It may be due to the hindered accessibility of this α-end carboxylic acid screened by the PEO brush.

As a conclusion, PEO-*b*-PAA or P(AA-*co*-PEOA) fluorescent core-shell nanoparticles can easily be functionalized, with the same grafting efficiency, with organic amines such as fluoresceinamine.

Conclusions

Several core-shell nanoparticles with a hydrophobic core made of polystyrene and a hydrophilic shell of P(AA-*co*-PEOA) copolymers have been synthesized *via* a RAFT miniemulsion process in water. It was shown that the nature and molar mass of the hydrophilic shell have a major impact on the control of the polymerization, as well as on the size and shape of the nanoparticles. Using pure PPEOA macro-RAFT agent in the polymerization process, particles with a void in their center, *i.e.* nanocapsules, were obtained, while pure PAA led to full nanoparticles. With P(AA-*co*-PEOA) random copolymers, either full particles or nanocapsules were formed, depending on their molar mass. To our knowledge this is the first time that nanoparticles with a shell of *comb-like* PAA and PPEOA were synthesized *via* a miniemulsion process without adding any surfactant. After having established the polymerization conditions for three types of core-shell nanoparticles with a shell of $PPEOA_{11}$, P(AA_6-*co*-$PEOA_6$) or P(AA_{11}-*co*-$PEOA_{11}$), the corresponding fluorescent nanoparticles with the same particle morphology could be synthesized. It appeared that the incorporation of 1 mol % of fluorophore (about 5 wt%) did not change the size of the particles and did not disturb the control of the polymerization. The obtained fluorescent nanoparticles of a mean diameter of ≈ 80 nm are approximately 1500 times brighter than a single fluorophore, are 100-1000 brighter than CdSe/CdS Quantum dots (based on estimated brightness) and are among the brightest polymer-based fluorescent nanoparticles. In addition, it appeared that nanoparticles with a bulky comb-like shell of P(AA-*co*-PEOA) were more fluorescent than particles with a linear shell of PEO-*b*-PAA analyzed in a previous study, while using less fluorescent monomer during the synthesis. This was attributed to the fact that FNPs with brush shells of PPEOA exhibit less carboxylic acid close to the BODIPY monomers and, in addition, possess a lower aggregation number, which may limit BODIPY aggregation. We think that this result is really promising in terms of chemicals economy and time-saving. Moreover, those nanoparticles that have a void in their middle (nanocapsules) could be of interest for the encapsulation of hydrophilic drugs or active molecules. At last, the possibility to graft amine-based pH-sensitive molecules, such as fluoresceinamine, on the nanoparticles was tested. *Comb-like* P(AA-*co*-PEOA) and *linear* PEO-*b*-PAA copolymers could be successfully grafted with fluorescein. For P(AA-*co*-PEOA) core-shell nanoparticles, it was possible to introduce 520 FA and 1960 BODIPY on the same nanoparticles. The same kind of nanoparticles with only FA on the shell and no π in the core have already successfully been used in order to monitor the growth *of Escherichia Coli* bacteria.[59] First, it was shown that FNPs did not disturb the growth of the bacteria. Furthermore, they were successfully used to accurately monitor the early development of bacteria in the presence or absence of antibiotics. In this context, we believe that the combination of two fluorophores in those nanoparticles can be even more powerful to design ratiometric sensors for cell detection and quantification.

Acknowledgements

The authors thank Bernadette Charleux (Univ. Lyon I, CPE Lyon, C2P2, LCPP) for her support on the project and the warm and productive discussions they add together. The authors also thank Gaëlle Pembouong (UPMC, LCP) for technical support on SEC analyses, Arnaud Brosseau (ENS Cachan, PPSM) for technical support on fluorescence spectroscopy measurements

and Min-Hui Li and Sabrina Hocine (Curie Institute, Laboratoire Physico-Chimie Curie, France) for zeta potential measurements.

Notes and references

‡ The diameter of the core of the FNPs is estimated by TEM (D_{TEM}, Table 2). Indeed, by electron microscopy, only the dense electronic structures as polystyrene can be observed. The less dense structure of the shell as poly(ethylene glycol) and poly(acrylic acid) can't been seen.

1 Louie, A. *Chem. Rev.* 2010, **110**, 3146–3195.
2 Hu, J., Liu, S. *Macromolecules,* 2010, **43**, 8315–8330.
3 Resch-Genger, U., Grabolle, M., Cavaliere-Jaricot, S., Nitschke, R., Nann, T. *Nat. Methods,* 2008, **5**, 763 – 775.
4 Chen, G., Roy, I., Yang, C., Prasad, P. N. *Chem. Rev.* 2016, acs.chemrev.5b00148.
5 Michalet, X., Pinaud, F. F., Bentolila, L. A., Tsay, J. M., Doose, S., Li, J. J., Sundaresan, G., Wu, A. M., Gambhir, S. S., Weiss, S. *Science,* 2005, **307**, 538–544.
6 Bonacchi, S., Genovese, D., Juris, R., Montalti, M., Prodi, L., Rampazzo, E., Zaccheroni, N. *Angew. Chemie - Int. Ed.,* 2011, **50**, 4056–4066.
7 Robin, M. P., O'Reilly, R. K. *Polym. Int.* 2015, *64*, 174–182.
8 Li, C., Zhang, Y., Hu, J., Cheng, J., Liu, S. *Angew. Chemie - Int. Ed.,* 2010, **49**, 5120–5124.
9 Breul, A. M., Hager, M. D., Schubert, U. S. *Chem. Soc. Rev.,* 2013, **42**, 5366–407.
10 Reisch, A., Klymchenko, A. S. *Small,* 2016, 10.1002/smll.201503396
11 Tasso, M., Giovanelli, E., Zala, D., Bouccara, S., Fragola, A., Hanafi, M., Lenkei, Z., Pons, T., Lequeux, N. *ACS Nano,* 2015, **9**, 11479–11489.
12 Cobo, I., Li, M., Sumerlin, B. S., Perrier, S. *Nat. Mater.,* 2015, **14**, 143–159.
13 Torchilin, V. *Adv. Drug Deliv. Rev.,* 2006, **58**, 1532–1555.
14 Sapsford, K. E., Algar, W. R., Berti, L., Gemmill, K. B., Casey, B. J., Oh, E., Stewart, M. H., Medintz, I. L. *Chem. Rev.,* 2013, **113**, 1904–2074.
15 Banerjee, A., Grazon, C., Nadal, B., Pons, T., Krishnan, Y., Dubertret, B. *Bioconjug. Chem.,* 2015, **26**, 1582–1589.
16 Delaittre, G., Greiner, A. M., Pauloehrl, T., Bastmeyer, M., Barner-Kowollik, C. *Soft Matter,* 2012, **8**, 7323.
17 Zetterlund, P. B., Kagawa, Y., Okubo, M. *Chem. Rev.,* 2008, **108**, 3747–3794.
18 Zetterlund, P. B., Thickett, S. C., Perrier, S., Bourgeat-Lami, E., Lansalot, M. *Chem. Rev.,* 2015, **115**, 9745–9800.
19 Sun, J.-T., Hong, C.-Y., Pan, C.-Y. *Polym. Chem.,* 2013, **4**, 873–881.
20 Charleux, B., Delaittre, G., Rieger, J., D'Agosto, F. *Macromolecules,* 2012, **45**, 6753–6765.
21 Rieger, J. *Macromol. Rapid Commun.* 2015, ***36***, 1458–1471.
22 Lansalot, M.; Rieger, J.; D'Agosto, F. Macromolecular self-assembly, *ISBN: 978-1-118-88712-7*; Wiley-VCH, Ed. O. Borisov and L. Billon, 2016; p. 45.
23 Canning S. L., Smith G. N. , Armes S. P., *Macromolecules*, 2016, **49**, 1985−2001.
24 Karagoz, B., Boyer, C., Davis, T. P. *Macromol. Rapid Commun.,* 2014, **35**, 417–21.
25 Zhou, W., Qu, Q., Xu, Y., An, Z. *ACS Macro Lett,.* 2015, **4**, 495–499.
26 Grazon, C., Rieger, J., Méallet-Renault, R., Clavier, G., Charleux, B. *Macromol. Rapid Commun.,* 2011, **32**, 699–705.
27 Knop, K., Hoogenboom, R., Fischer, D., Schubert, U. S. *Angew. Chemie - Int. Ed.,* 2010, **49**, 6288–6308.
28 Schork, F. J., Luo, Y., Smulders, W., Russum, J. P., Butté, A., Fontenot, K. *Adv. Polym. Sci.,* 2005, **175**, 129–255.
29 Chen, J., Zhong, W., Tang, Y., Wu, Z., Li, Y., Yi, P., Jiang, J. *Macromolecules,* 2015, **48**, 3500–3508.
30 Pham, B. T. T., Nguyen, D., Ferguson, C. J., Hawkett, B. S., Serelis, A. K., Such, C. H. *Macromolecules,* 2003, **36**, 8907–8909.
31 Pham, B. T. T., Zondanos, H., Such, C. H., Warr, G. G., Hawkett, B. S. *Macromolecules,* 2010, **43**, 7950–7957.
32 Rieger, J., Stoffelbach, F., Bui, C., Alaimo, D., Jérôme, C., Charleux, B. *Macromolecules,* 2008, **41**, 4065–4068.
33 Santos, a. M. Dos, Bris, T. Le, Graillat, C., D'Agosto, F., Lansalot, M. *Macromolecules,* 2009, **42**, 946–956.
34 Wang, X., Luo, Y., Li, B., Zhu, S. *Macromolecules,* 2009, **42**, 6414–6421.
35 Chaduc, I., Crepet, A., Boyron, O., Charleux, B., D'Agosto, F., Lansalot, M. *Macromolecules,* 2013, **46**, 6013–6023.
36 Boissé, S., Rieger, J., Belal, K., Di-Cicco, A., Beaunier, P., Li, M.-H., Charleux, B. *Chem. Commun.,* 2010, *46*, 1950–1952.
37 Tan, J., Rao, X., Yang, J., Zeng, Z. *Macromolecules,* 2013, **46**, 8441–8448.
38 Zhu, Y., Bi, S., Gao, X., Luo, Y. *Macromol. React. Eng.,* 2015.
39 Zhang, X., Boissé, S., Zhang, W., Beaunier, P., D'Agosto, F., Rieger, J., Charleux, B. *Macromolecules,* 2011, **44**, 4149–4158.
40 Zhang, W., D'Agosto, F., Dugas, P. Y., Rieger, J., Charleux, B. *Polymer,* 2013, **54**, 2011–2019.
41 Boursier, T., Chaduc, I., Rieger, J., D'Agosto, F., Lansalot, M., Charleux, B. *Polym. Chem.,* 2011, **2**, 355-362.
42 Couvreur, L., Lefay, C., Belleney, J., Charleux, B., Guerret, O., Magnet, S. *Macromolecules,* 2003, **36**, 8260–8267.
43 Kubin, R., Fletcher, A. *J. Lumin.,* 1982, **27**, 455–462.
44 Bernard, V. *Molecular fluorescence, Principles and Applications*, Wiley-VCH: Weinheim, Germany, 2002.
45 Grazon, C., Rieger, J., Méallet-Renault, R., Charleux, B., Clavier, G. *Macromolecules,* 2013, **46**, 5167–5176.
46 Carvell, M., Robb, I. D., Small, P. W. *Polymer,* 1998, **39**, 393–398.
47 Luo, Y., Wang, X., Li, B. G., Zhu, S. *Macromolecules,* 2011, **44**, 221–229.
48 Lesage de la Haye J., Zhang X., Chaduc I., Brunel F., Lansalot M. D'Agosto F., *Angew. Chemie - Int. Ed.* 2016*,* **55***,* 3739-3743.
49 Sun, J.-T., Hong, C.-Y., Pan, C.-Y. *Soft Matter,* 2012, *8*, 7753.
50 Zhang, W., D'Agosto, F., Boyron, O., Rieger, J., Charleux, B. *Macromolecules,* 2011, **44**, 7584–7593.
51 Boens, N., Wang, L., Leen, V., Yuan, P., Verbelen, B., Dehaen, W., Van Der Auweraer, M., De Borggraeve, W. D., Van Meervelt, L., Jacobs, J., Beljonne, D., Tonnelé, C., Lazzaroni, R., Ruedas-Rama, M. J., Orte, A., Crovetto, L., Talavera, E. M., Alvarez-Pez, J. M. *J. Phys. Chem. A,* 2014, **118**, 1576–1594.
52 Grazon, C., Rieger, J., Charleux, B., Clavier, G., Méallet-Renault, R. *J. Phys. Chem. C,* 2014, **118**, 13945–13952.
53 Qin, W., Rohand, T., Dehaen, W., Clifford, J. N., Driesen, K., Beljonne, D., Van Averbeke, B., Van Auweraer, M. Der, Boens, N. *J. Phys. Chem. A,* 2007, **111**, 8588–8597.
54 Delaittre, G., Justribõ-Hernández, G., Nolte, R. J. M., Cornelissen, J. J. L. M. *Macromol. Rapid Commun.,* 2011, **32**, 19–24.
55 Akkahat, P., Mekboonsonglarp, W., Kiatkamjornwong, S., Hoven, V. P. *Langmuir,* 2012, **28**, 5302–5311.
56 Meng, F., Engbers, G. H. M., Feijen, J. *J. Biomed. Mater. Res. A,* 2004, **70**, 49–58.
57 Yang, S., Yu, X., Wang, L., Tu, Y., Zheng, J. X., Xu, J., Van Horn, R. M., Cheng, S. Z. D. *Macromolecules* ,2010, **43**, 3018–3026.

58 Grazon, C. Elaboration de nanoparticules fluorescentes à base de BODIPY par polymérisation RAFT en miniemulsion, Ecole Normale Supérieure de Cachan, France.
59 Si, Y., Grazon, C., Clavier, G., Rieger, J., Audibert, J.-F., Sclavi, B., Méallet-Renault, R. *Biosens. Bioelectron.,* 2016, **75**, 320–327.